Journal of Materials Chemistry C

ROYAL SOCIETY OF CHEMISTRY

PAPER

View Article Online
View Journal | View Issue

Cite this: J. Mater. Chem. C, 2026, 14, 1260

Competition between helical and heliconical twist in the development of complex soft matter structures

Büşra Yıldız Özdemir, [a] Aykun Özkonstanyan, [a] Christian Anders,[b] Demet Karaca Balta, [a] Hale Ocak Gümrükçü, *[a] Carsten Tschierske *[b] and Mohamed Alaasar *[bc]

Received 8th September 2025,
Accepted 19th November 2025

DOI: 10.1039/d5tc03348a

rsc.li/materials-c

Chirality strongly influences the self-assembly of soft matter systems, yielding new superstructures with numerous potential applications. Here, two series of 4-cyanoresorcinol-based bent-core liquid crystals (BCLCs) in which molecular chirality is provided by the introduction of a branched (*S*)-2-alkyloxypropyl end chain at both or only one end of the aromatic core have been synthesized and characterized to study the effects of chain branching and molecular chirality on liquid crystalline (LC) self-assembly. Two new LC phases with tilted and twisted arrangements of the molecules, restricted rotation around the long axis, preferred face-to-face stacking of the polyaromatic cores, and only a short correlation length of lamellar ordering were discovered; one is achiral and isotropic (M_{Iso}) while the other is chiral and low birefringent (M_L*). With decreasing density of the chain branching (*i.e.*, stereogenic centers), the achiral M_{Iso} phase is replaced by the birefringent heliconical M_L* phase, an amorphous type III blue phase (BPIII), a heliconical tilted smectic phase (SmC*), and a chiral cybotactic nematic phase composed of SmC* clusters (N_{CybC}*). In this N_{CybC}* phase, the twist is heliconical, in contrast to the conventional non-cybotactic chiral nematics where it is helical. The heliconical twist is favored and the helical twist is suppressed by the emergence and growth of SmC-type cybotactic clusters. At the transition to a denser, face-to-face-packed core, saddle-splay emerges, and helical twist can become stronger, supporting layer deformation and causing a transition from the heliconical SmC* *via* M_L* to the achiral M_{Iso} phase as the density of chain-branched stereogenic centers increases and temperature decreases.

1. Introduction

Liquid crystals (LCs) represent intermediate states of matter between crystalline solids and isotropic liquids.[1–3] As such, they can simultaneously exhibit the long-range order and the anisotropic properties of crystalline solids and the flow properties of isotropic liquids, *i.e.*, the molecules rotate and move as in liquids, while maintaining long-range orientational and/or positional order. This combination of order and mobility leads to unique properties of LCs, such as self-healing, adaptability and responsiveness to external stimuli, making them excellent candidates for technological uses, for example, as materials in optical, electrooptical and photonic devices,[4,5] for sensing applications,[6] as charge carrier materials in organic field effect transistors (OFETs), organic light emitting diodes (OLEDs), organic photovoltaics (OPVs),[7–9] and for ion transportation.[10]

According to the molecular shape, the LC compounds can be divided into calamitic (rod-like), disc-like, and bent-core molecules, which have specific geometries as required for the formation of thermotropic lamellar, columnar, and cubic LC phases.[1–3,11] Among them, the bent-core (BC) molecules are distinct by a rich mesomorphism, their ability to show antiferroelectric or ferroelectric switching[12–17] and their capability of spontaneous mirror symmetry breaking.[14,15,18–21] Moreover, BC liquid crystals (BCLCs) often exhibit non-cubic optically isotropic mesophases. Their formation is supported by an intrinsic frustration of the packing of bent molecules in flat layers, leading to the development of saddle splay and sponge-like layer deformation (Fig. 1(b) and (c)).[22] In many of these isotropic mesophases, spontaneous mirror symmetry breaking can be detected by polarizing optical microscopy (POM) between polarizers, if these polarizers are slightly twisted either clockwise or anticlockwise out of the 90° crossed

[a] Yildiz Technical University, Department of Chemistry, 34220 Esenler, Istanbul, Turkey. E-mail: hocak@yildiz.edu.tr
[b] Institute of Chemistry, Organic Chemistry, Martin Luther University Halle-Wittenberg, Kurt-Mothes-Str. 2, D-06120 Halle, Germany. E-mail: carsten.tschierske@chemie.uni-halle.de, mohamed.alaasar@chemie.uni-halle.de
[c] Department of Chemistry, Faculty of Science, Cairo University, 12613 Giza, Egypt

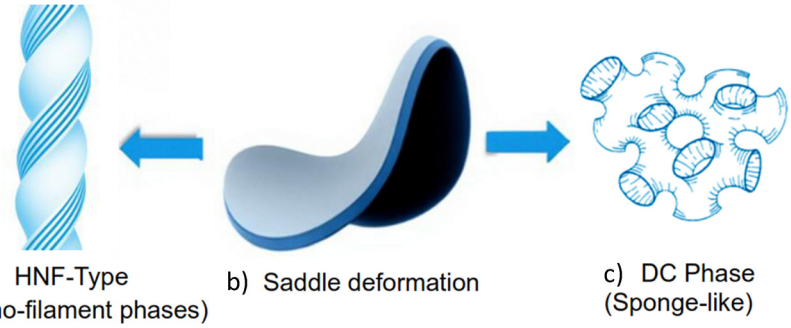

Fig. 1 Saddle-deformed layers (b) assemble either to (a) the soft crystalline HNF-type phases or c) the fluid sponge-like DC phases.

orientation.[14,15,19] Typically, the development of conglomerates of oppositely chiral domains (dark conglomerate phases, DC phases) is observed in these isotropic mesophases of achiral BCLCs, indicating ambidextrous mirror symmetry breaking.[18–20,22,23]

Superstructural chirality[24] can arise due to the development of a uniform twist between the molecules with the formation of helical assemblies,[14,19] which could be further supported by the transient chirality of the molecular conformations provided by the semiflexible polyaromatic core structures.[18,19,25] There are two distinct modes of superstructural helix formation. The helical twist can take place by rotation of the molecular long axes around a helix axis (Fig. 2(a) and (b)), while the heliconical twist takes place by precession of the molecules on a cone around the helix axis (Fig. 2(c) and (d)). In nematic phases of uniformly chiral molecules, the twist is helical (cholesteric phases, N*, Fig. 2(a))[26] and only in twist-bend nematic (N_{TB})[27–29] and ferroelectric nematic phases (N_F)[30] of achiral molecules heliconical twist was observed (Fig. 2(c)). In lamellar phases, the heliconical twist is preferred, because in this case the helix axis develops along the layer normal, which does not distort the layers (Fig. 2(d)).[26] However, in the case of helical twist, the helix axis develops parallel to the layer planes which distorts the layers and supports layer deformation into helical ribbons (Fig. 1(a) and 2(b)) or – in a more disordered way – into sponge-like deformed structures (Fig. 1(c)). If this helical distortion becomes sufficiently strong, or it is combined with other layer distorting effects, then the LC phases can lose long range order and anisotropic properties and thus become optically isotropic. The development of a superstructural chirality due to helical twist can be spontaneous for achiral compounds, leading to a conglomerate of chiral domains (ambidextrous symmetry breaking) or induced for nonracemic chiral compounds, then leading to a preferred twist/chirality sense.

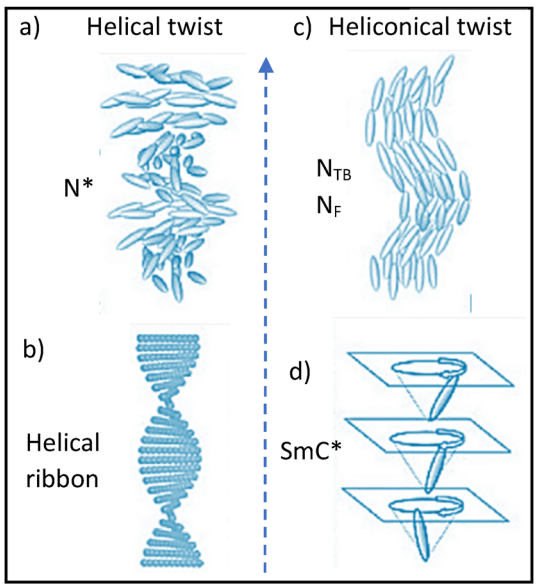

Fig. 2 Helical and heliconical twist in LC phases: (a) and (b) helical is the uniform twist of the molecular long axis around a helix axis (dashed arrow) while (c) and (d) heliconical twist takes place by precession of the tilt direction on a cone around the helix axis, occurring either in (a) and (c) nematic phases, or in (b) and (d) lamellar aggregates or smectic phases.

For achiral BCLCs, there are two major types of isotropic mesophases (Fig. 1). The first is formed by sponge-like deformed fluid layers (sponge phases, Fig. 1(c)),[22,31–36] or fragments of layers (random grain boundary phases = RGB[37]). The second one is observed if the molecules are organized in stacks of semicrystalline twisted ribbons forming arrays of helical nano-scale filaments (HNF phases or B4 phases, Fig. 1(a)),[23,38–41] which can be further fragmented into smaller helical nano-crystallites (HNC[42]) or fused to heliconical nanocylinders (HLNC[40]). Additional mesophases with or without expression of superstructural chirality were found at the transition between the fluid DC and soft crystalline HNF types.[43–45]

Molecular chirality has a huge effect on LC phases by supporting the development of uniform helical or heliconical twist, for example, leading to cholesteric phases, blue phases, and twist grain boundary phases.[14,15,17,46–49] The effects of permanent chirality were also studied for the ambidextrous chiral DC-type[50–53] and HNF-type phases of BCLCs.[54–57] Here, the molecular chirality can induce uniform chirality by chirality amplification,[19] but remarkably, there are also cases where it is obviously incapable of dominating the chirality sense of the superstructures, retaining an overall racemic (achiral)[58] or ambidextrous chiral conglomerate structure of the isotropic mesophases.[53]

One of the most promising central core units used in designing BCLCs is the 4-cyanoresorcinol core (Scheme 1(a)), where the lateral CN group at the apex provides polarity and a

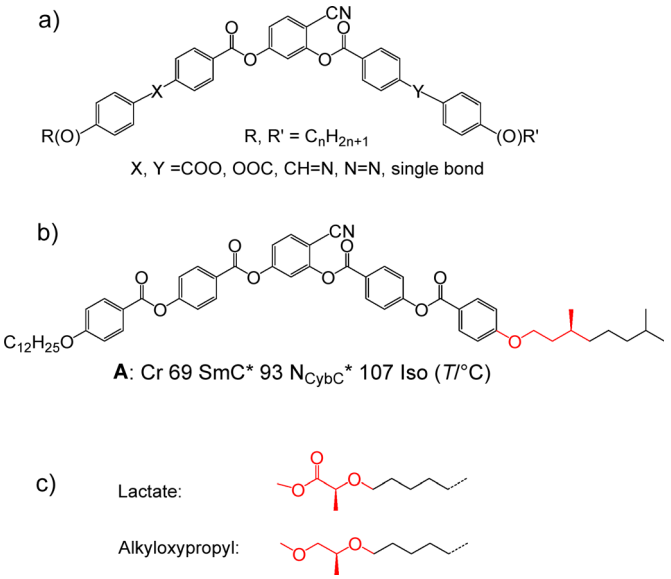

Scheme 1 (a) General structure of 4-cyanoresorcinol-derived BCLCs; (b) example of a chiral 4-cyanoresorcinol-based BCLC with phenylbenzoate wings and a branched alkyl chain derived from (*S*)-dihydrocitronellol (compound **A**) and its transition temperatures,[79] and (c) the structures of the lactate and 2-alkoxypropyloxy derived chiral groups with (*S*)-configuration.

reduced molecular bending (~110°) compared to other BCLCs with ~120°, due to its effect on the conformation of the neighboring COO group.[59–61] These 4-cyanoresorcinol-based BCLCs display cybotactic nematic (N_{CybA}, N_{CybC}),[62,63] apolar, paraelectric (SmA, SmC), polarization randomized ($SmAP_R$, $SmCP_R$[64]) and antiferroelectric smectic ($SmAP_A$,[65] $SmCP_A$) phases, depending on temperature and length of the alkyl end-chains R and R′,[66] while the linking units X and Y have a significant effect on the development of tilt and its correlation between the layers, being absent or de-Vries-like randomized in SmA,[67] heliconical twisted $(Sm(CP)^{hel})$,[68–71] anticlinic tilted (SmC_a) or synclinic tilted (SmC_s) between adjacent layers.[61,72–75]

The effect of molecular chirality on LC phases of 4-cyanoresorcinol-based BCLCs has been studied previously with branched alkyl chains (see, for example, compound **A** in Scheme 1(b)).[76–80] However, the helical twisting power (HTP) and other chirality effects are relatively weak for branched alkyl chains,[47] while non-carbon heteroatoms at the stereogenic center, as found in lactates,[81–84] and related 2-alkyloxypropyl ethers (Scheme 1(c)), tend to increase these chirality effects. While lactates have rarely been used for BCLCs,[85] the 2-alkyloxypropyl group has not been combined with bent cores and was only reported for a few rod-like LCs in patents for application in mixtures for the display industry.[86]

Here, we report the synthesis and characterization of new symmetric and non-symmetric bent-core liquid crystals, in which the molecular chirality is provided by the introduction of the uniformly chiral (*S*)-2-alkyloxypropyl terminal group at both ends or at only one end of a polyaromatic bent-core structure derived from the 4-cyanoresorcinol unit with two phenyl benzoate wings (compounds **I** and **II** in Scheme 2). The present study is focused on investigating the influence of the number of stereogenic centers and the effects of alkyl chain length on the soft self-assembly in chirality-modulated LC phases. This work provides two new mesophases, an achiral optically isotropic mesophase (M_{Iso}) and a chiral low birefringent mesophase (M_L*). The latter is accompanied by an amorphous blue phase (BPIII), and birefringent cybotactic nematic (N_{CybC}*) and SmC* phases. In contrast to conventional helical nematic (cholesteric, N*) phases of chiral rod-like compounds, the twist in the N_{CybC}* phase is heliconical (Fig. 2(c)).[47] Overall, this work contributes to the understanding of the development of isotropic mesophases and the effects of helical and heliconical twist on LC self-assembly of weakly bent molecules.

2. Experimental

2.1. Synthesis

The target compounds **Ia-c** and **IIa-c** were synthesized as shown in Scheme 3. The homochiral benzoic acids (**7a-c**) were synthesized as described in Scheme S1 from (*S*)-ethyl lactate (optical rotation: $\propto_D^{20}$ −10.5 ± 1°, neat, ≥99 : 1 enantiomeric ratio (GC), Sigma Aldrich). Alkylation with the appropriate alkyl iodides was conducted with Ag_2O to retain the configuration and to avoid any racemization.[87] The *O*-alkyl substituted ethyl lactates were then reduced to the (*S*)-2-alkyloxypropanols with $LiAlH_4$, followed by tosylation.[87] The obtained 4-((*S*)-2-alkyloxypropyloxy)tosylates were used for the following steps of the synthesis of compounds **7a-c**, as outlined in more detail in

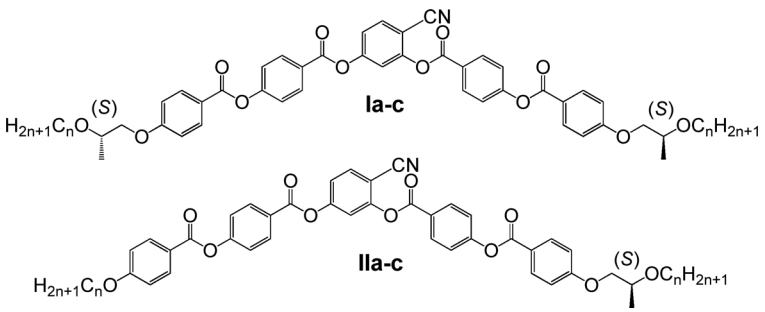

Scheme 2 Structures of the chiral compounds **I** and **II** under investigation.

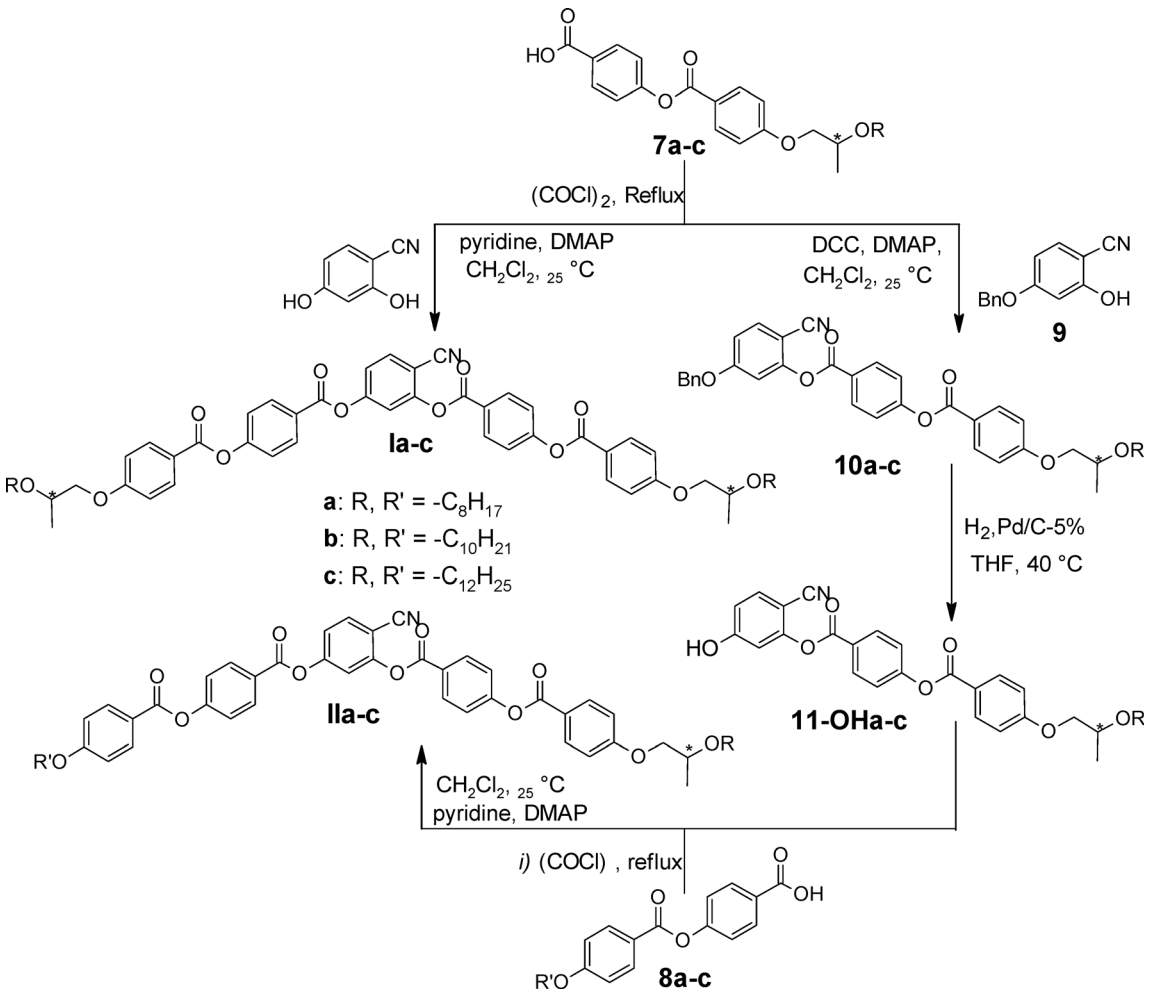

Scheme 3 Synthesis of the target bent-core molecules **Ia-c** and **IIa-c**.

Scheme S1. This sequence of reactions was previously proven to retain the stereochemical integrity.[87] The achiral acids **8a-c** were synthesized using the same procedure as reported in ref. 88. The benzoic acids **7a-c** and **8a-c**[79,80] were converted to their corresponding acid chlorides using oxalyl chloride.[89] The central bent-core units 2,4-dihydroxybenzonitrile[90] and 4-benzyloxy-2-hydroxybenzonitrile[90] were synthesized according to previously reported procedures.[59,62,77,80]

For the synthesis of the symmetric compounds **Ia-c**, the 4-(4-((*S*)-2-alkoxypropyloxy)benzoyloxy)benzoic acids **7a-c** (n = 8, 10, 12) were first reacted with oxalyl chloride to give the corresponding benzoyl chlorides. Then, the esterification reaction between two equivalents of the corresponding benzoyl chlorides and 2,4-dihydroxybenzonitrile was carried out by using DMAP and dry pyridine as a base in dry dichloromethane, as reported earlier.[85] For the synthesis of the non-symmetric compounds **IIa-c**, 4-benzyloxy-2-hydroxybenzonitrile **9** was acylated with one equivalent of the benzoic acids **7a-c** using DCC.[91] Then, the benzyl group was removed by a deprotection by hydrogenation using Pd/C-5% as a catalyst.[80] Finally, the acylation of the obtained phenols **11-OHa-c** with the 4-(4-*n*-alkyloxybenzoyloxy)benzoyl chlorides **8a-c**, resulted in compounds **IIa-c**. The detailed synthetic procedure, the spectroscopic data of intermediates as well as final compounds **Ia-c** and **IIa-c** are provided in the SI.

2.2. Investigations

The liquid crystalline properties of bent-core molecules **Ia-c** and **IIa-c** were investigated by using POM and differential scanning calorimetry (DSC), and the bent-core compounds were additionally studied by means of small- and wide-angle X-ray scattering (SAXS, WAXS). The methods and the equipment used are described in the SI.

3. Results and discussion

3.1. Self-assembly of compounds Ia-c with two branched chains: isotropic mesophases M_{Iso}

The phase transitions of the bent-core compounds **Ia-c** are given in Table 1. The DSC traces of compounds **Ib** and **Ic** with two (*S*)-2-*n*-alkyloxypropyl terminal chains show only one endotherm on heating and one exotherm upon cooling with relatively high enthalpies of 12–16 kJ mol^{-1} (see Fig. 3(a) and

Table 1 Mesophase types, phase transition temperatures, and corresponding enthalpy values of compounds **Ia-c**[a]

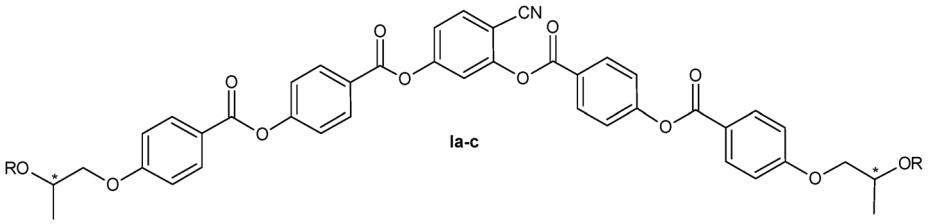

Compd.	R	L_{mol}/nm	T/°C [ΔH/kJmol^{-1}]	d/nm[b] (T/°C)
Ia	$-C_8H_{17}$	5.0	**H:** M_{Iso} 47 [*16.0*] Iso **C:** Iso ~15 [*6.4*] M_{Iso}	4.4–4.5 (30)
Ib	$-C_{10}H_{21}$	5.5	**H:** M_{Iso} 53 [*17.1*] Iso **C:** Iso 30 [*−16.0*] M_{Iso}	4.6 (29)
Ic	$-C_{12}H_{25}$	6.0	**H:** M_{Iso} 53 [*12.3*] Iso **C:** Iso 33 [*−11.6*] M_{Iso}	4.8 (40)

[a] Peak temperatures, taken from 2nd heating (**H**) and cooling (**C**) scans at 10 K min^{-1}; abbreviations: M_{Iso} = isotropic mesophase, Iso = isotropic liquid phase; L_{mol} is measured with a 120 °C angle of the molecular bend and maximal stretched chains, for more X-ray data and correlation lengths, see Tables S2, S3 and Fig. S49–S51. [b] In the M_{Iso} phase.

Fig. S44a, b), being in the typical range for LC-Iso transitions of bent-core mesogens.[14] Upon cooling compounds **Ia-c** below the phase transition, the viscosity increases, while the optical isotropy is retained (M_{Iso}). Even by shearing the sample, no birefringence can be induced in this viscoelastic isotropic mesophase, and no field-induced birefringence was observed in electro-optical experiments (applied field strength up to 38 V μm^{-1}). This means that no birefringent phase can be field-induced, as observed for other cases of isotropic mesophases of bent-core mesogens.[14,19,22] For further investigation of the M_{Iso} phase, small-angle and wide-angle X-ray scattering (SAXS and WAXS) were performed. As expected, there is only diffuse scattering in the isotropic liquid state (Iso), with one maximum located for **Ia** at d = 3.2–3.4 nm (Fig. 3(c), red curve) and the other one at 0.46 nm (Fig. S49b and c). At the transition to M_{Iso} the SAXS increases in intensity, becomes a bit narrower, and is shifted to larger distances (d = 4.4 nm, Fig. 3(c)), in line with a transition from the disordered liquid to a more ordered phase. No indication of any additional scattering can be detected, which excludes a cubic lattice or an HNF-like structure for M_{Iso}. From the line width at half maximum (FWHM), a longitudinal correlation length of L_ζ ~ 10–11 nm (Table S2), corresponding to only twice the molecular length, is estimated, typical for a highly disordered structure, which is responsible for the absence of birefringence. Hence, there is only local, but no long-range periodic order in the M_{Iso} phase. For **Ib** and **Ic**, the d-values of the SAXS scattering are d = 4.6 nm and d = 4.8 nm (in all cases being a bit smaller than the expanded molecular length (L_{mol} = 5.0, 5.5, and 6.0 nm for **Ia**, **Ib**, and **Ic**, respectively, see Table 1 and Fig. S50, S51). If a lamellar organization is assumed as the fundamental organization mode, then the polyaromatic cores are likely to be tilted. The d/L_{mol} ratios slightly decrease with growing chain length from ~0.9 *via* 0.84 to 0.8, indicating either an increasing tilt and a growing contribution of chain folding or partial chain intercalation to the reduction of the layer distance. As no aligned samples could be obtained for this isotropic mesophase with a distorted structure, a direct confirmation of the tilt by XRD was not possible. Nevertheless, the presence of tilt is the most likely option, because similar molecules with the same core structure based on a slightly bent 4-cyanoresorcinol core with two phenyl benzoate wings show in all previously reported cases exclusively tilted LC phase ($SmCP_A$, SmC, N_{CybC}).[60,62] For example, compound **A** (Scheme 1(b)) with the same core unit, the same molecular length (L_{mol} = 5.0 nm) and the same number of chain branching as **Ia** has a SmC phase with d = 4.6 nm at 70 °C,[79] which is even a bit larger than the value of d = 4.4–4.5 nm measured for the M_{Iso} phase of **Ia**. This supports a tilted organization of the molecules in distorted layers for M_{Iso}.

The wide-angle scattering in the M_{Iso} ranges of compounds **Ia-c** remains diffuse with a maximum around 0.45–0.46 nm as typical for liquids and LCs, but with additional diffuse shoulders at larger and smaller 2θ values in all three cases (Fig. 3(d), Fig. S49b, S50b, and Table S2). For compound **Ic** (Fig. 3(d)), for example, one shoulder is located at d = 0.36 nm, being the typical π-stacking distance between face-to-face arranged aromatics. The other weaker shoulder at smaller 2θ-values has a larger distance of d = 0.62 nm, corresponding approximately to the edge-to-edge distance between benzene rings. We attribute the main scattering around 0.46 nm to the mean lateral distance between the disordered alkyl chains, and the two additional shoulders to a face-to-face and edge-to-edge packing of the polyaromatic cores in nano-segregated lamella involving the tilted and parallel aligned polyaromatic cores (Fig. 3(e) and (f)).

There is a similarity in the shape of the WAXS to that reported for a birefringent, *i.e.* non-distorted, tilted lamellar LC phase of diazaazulene-based LCs (DAA, see Fig. S55 for structure), where the analysis of aligned samples confirmed a synclinic tilted organization with a face-to-face packing of the polyaromatic cores (Col_L), as shown in Fig. 3(e).[92] It is likely that in the M_{Iso} phase the local structure in the layers is similar

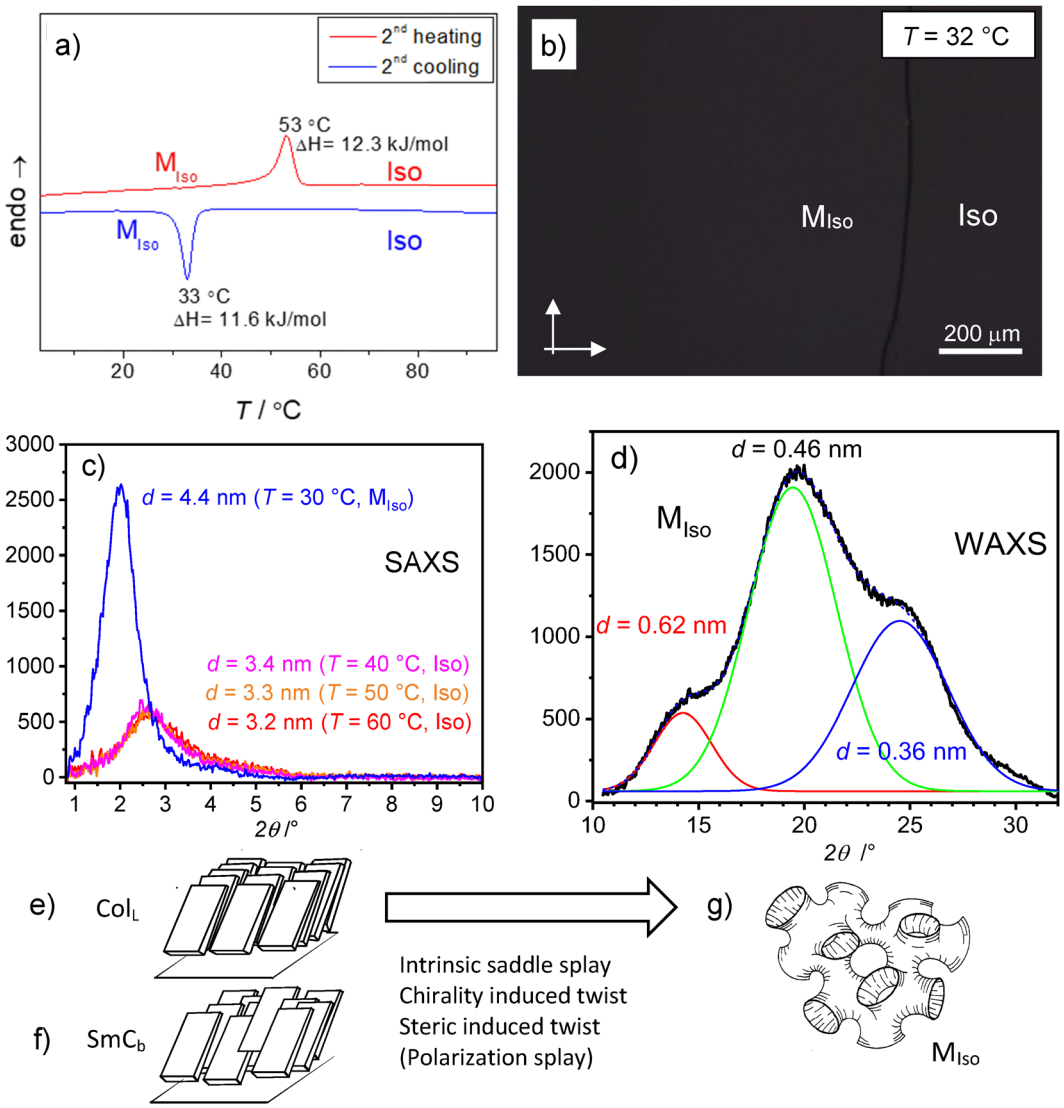

Fig. 3 Investigation of compounds **I**. (a) DSC thermograms of **Ic** on 2nd heating and cooling (10 K min^{-1}); (b) M_{Iso} phase of **Ic** as observed upon cooling between crossed polarizers (white arrows) in a 10 µm PI coated cell; (c) temperature dependence of the SAXS patterns of **Ia** as recorded on cooling (M_{Iso} = blue, Iso = reddish colors) and (d) WAXS pattern of **Ic** in the M_{Iso} phase at 30 °C with deconvolution into three curves; (e) and (f) show the local molecular organization proposed for the M_{Iso} phase with a tilted face-to-face packing of the tilted polyaromatic cores (Col_L/SmC_b), the difference between them is the correlation length of side-by-side ordering of the π-stacked molecules in the layers, (e) being long range in the lamellar columnar phase Col_L and (f) short range in the smectic SmC_b phase (C indicates the tilt while subscript b indicates the biaxiality due to restricted rotation); (g) shows the deformation of the layers into the sponge-like isotropic lamellar phase in M_{Iso}; for additional XRD scans see Fig. S49–S51; for numerical X-ray data and correlation lengths, see Tables S2 and S3.

and combines tilt with restricted rotation around the long axis in a smectic phase with face-to-face packing of the molecules. Because there is no additional SAXS reflection and all WAXSs are broad, there appears to be only some orientational correlation of the primary and secondary directors, but no positional correlation of the tilted molecules in the layers, as depicted in Fig. 3(f) (SmC_b-like local structure).

The optical isotropy, together with the short correlation length of smectic ordering, indicate the presence of a strong layer deformation. For bent-core molecules, saddle-splay deformation of the layer into a sponge-like structure is an often-observed phenomenon (Fig. 3(g)).[22] This is supported by chain branching, which expands the effective chain cross-section, thus favoring the development of curvature by splay and twist, the latter being additionally supported by molecular chirality.

Though the majority of known isotropic mesophases of (achiral) BCLCs show ambidextrous mirror symmetry breaking, in the M_{Iso} phases of the chiral compounds **Ia-c** no optical rotation can be detected by means of polarizing microscopy. Especially, no conglomerate texture can be observed, and the maximum extinction is in all M_{Iso} phases exactly at 90 (± 0.1)° crossed orientation between analyzer and polarizer, excluding uniform superstructural chirality (but not excluding a smaller optical rotation by molecular chirality, see discussion in

Section S5). Moreover, no selective reflection (in the range of the wavelength of visible light) can be observed as an indication of a photonic bend gap due to helical/heliconical self-assembly. Thus, there is no evidence of any superstructural chirality, while molecular chirality is proven by the induction of a cholesteric phase in an achiral nematic 5-CB host with only 1 mol% of **1b** as dopant (see Section S4 and Fig. S54). This means that either there is no chiral superstructure in the M_{Iso} phase, it cannot be detected by the used methods, or an achiral or racemic superstructure is formed despite the presence of uniform molecular chirality; this will be discussed in Section 3.4.

For all compounds **I** partial crystallization takes place only slowly after prolonged storage at room temperature (after several hours), as proven by POM by an emerging birefringence and by XRD (see, for example, Fig. S51b).

3.2. Self-assembly of bent-core compounds IIa-c: M_L* formation in competition with nematic ordering

Remarkably, the situation changes if chirality is ''diluted'', *i.e.*, if one of the chiral end-chains is replaced by an achiral linear alkyl chain in compounds **IIa-c** (Table 2, see also Tables S2 and S3). The DSC traces of the three compounds **IIa-c** are different and show an increasing number of phase transitions with growing chain length (Fig. 4 and Fig. S44c). Simultaneously, the LC-Iso transition temperature rises. In the DSC traces of all three compounds, there is a main transition with relatively high enthalpy, increasing with alkyl chain elongation (ΔH = 8–18 kJ mol^{-1}), and being in the same range as the enthalpy values observed for the M_{Iso}–Iso transitions in compounds **Ia-c**. Below this relatively broad transition, the fluid mesophases become viscous. As found for compounds **I**, all compounds **II** partially crystallize only after prolonged storage at or below room temperature.

3.2.1. Compound IIa with BPIII–M_{Iso} transition. Compound **IIa** with the shortest end-chains shows only one endotherm with a maximum at 56 °C, corresponding to the transition to the isotropic liquid state on heating and one exotherm with a maximum at 26 °C in the cooling run (Fig. 4(a)). Upon cooling, the sample remains optically isotropic in the whole investigated temperature range down to 20 °C. A faint bluish color appears at around 52 °C which becomes more prominent upon shearing (Fig. 5(a)), while the diffuse SAXS is shifted from d = 3.5 nm in Iso at 70 °C *via* 4.0 nm at 50 °C to 4.5 nm at 40 °C, accompanied by an increase of intensity and narrowing line width due to a growing correlation length L_ζ from 4.4 nm at 70 °C to 16.3 nm at 40 °C (from a single to about four molecular lengths Fig. 5(e) and Table S2). It appears that in this temperature range, lamellar clusters develop and grow. The WAXS remains diffused with a single scattering maximum at d = 0.45 nm in this temperature range (orange curve in Fig. 5(f)). Though the d-values are still shorter than the molecular length (L_{mol} = 4.6 nm), the difference between SAXS d-spacing and molecular length is the smallest among all investigated compounds. This is in line with a reduction of the tilt angle, as typically observed for related *n*-alkyl substituted 4-cyanoresorcinols with decreasing chain length.[60,62] Based on the XRD data and the bluish selective reflection of this isotropic mesophase, we consider this temperature range between ca 52 °C and the next phase transition at 26 °C as an amorphous BPIII-like phase with simultaneous helix formation in all three spatial dimensions, but without formation of a long-range lattice.[78,93–100] The transition from Iso to BPIII appears to be continuous (without a visible DSC peak) and is associated with an almost continuous growth of cybotactic clusters.

Upon further cooling, the bluish selective reflection suddenly disappears, and the sample becomes increasingly viscous around 32 °C at the onset of the DSC peak with a maximum at 26 °C (see Fig. 4(a) and 5(c), (d)). Below this temperature, the field of view in POM is completely dark with maximum darkness at a 90° angle between polarizer and analyzer (Fig. 5(c) and (d)), as also found for the M_{Iso} phase of compounds **Ia-c**. Around this temperature, the SAXS widens, leading to a

Table 2 Mesophase types, phase transition temperatures, and corresponding enthalpy values of compounds **IIa-c**[a]

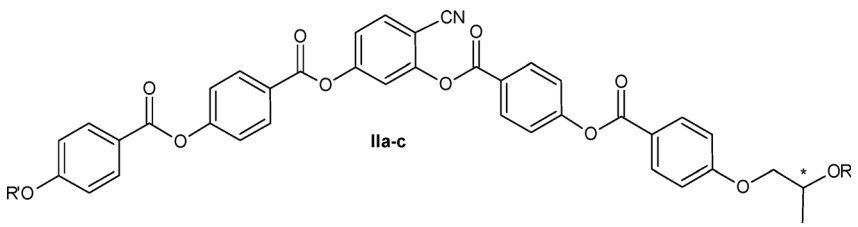

IIa-c

Compd.	R, R′	L_{mol}/nm	T/°C [ΔH/kJ mol^{-1}]	d/nm[c] (T/°C)
IIa	$-C_8H_{17}$	4.6	**H:** M_{Iso} 56 [*7.6*] Iso **C:** Iso 52 [—][b] BPIII 26 [*−5.2*] M_{Iso}	4.4 (40)
IIb	$-C_{10}H_{21}$	5.1	**H:** M_L* 60 [*14.7*] N_{CybC}* 80 [*0.8*] Iso **C:** Iso 76 [*−0.6*] N_{CybC}* 32 [*−11.1*] M_L*	4.7 (35)
IIc	$-C_{12}H_{25}$	5.6	**H:** M_L* 62 [*17.5*] SmC* 76 [*0.1*] N_{CybC}* 89 [*1.0*] Iso **C:** Iso 86 [*−1.3*] N_{CybC}* 74 [*−0.1*] SmC* 42 [*−15.8*] M_L*	5.2 (35)

[a] Peak temperatures and enthalpy values were taken from 2nd heating (**H**) and cooling (**C**) scans at 10 K min^{-1}. Abbreviations: BPIII = amorphous Blue Phase, N_{CybC}* heliconical cholesteric phase composed of SmC* clusters; for other abbreviations, see Table 1; for more XRD data and correlation lengths, see Tables S2, S3. [b] Transition was determined by POM. [c] SAXS in the M_{Iso} and M_L* phase.

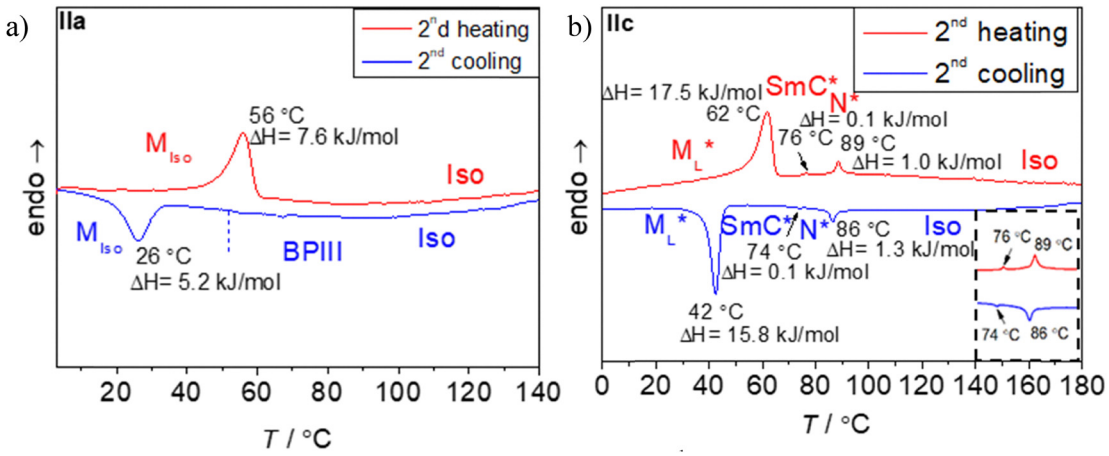

Fig. 4 DSC thermograms on 2nd heating and cooling (10 K min^{-1}) of (a) **IIa** and (b) **IIc**; see Fig. S44c for DSCs of **IIb**.

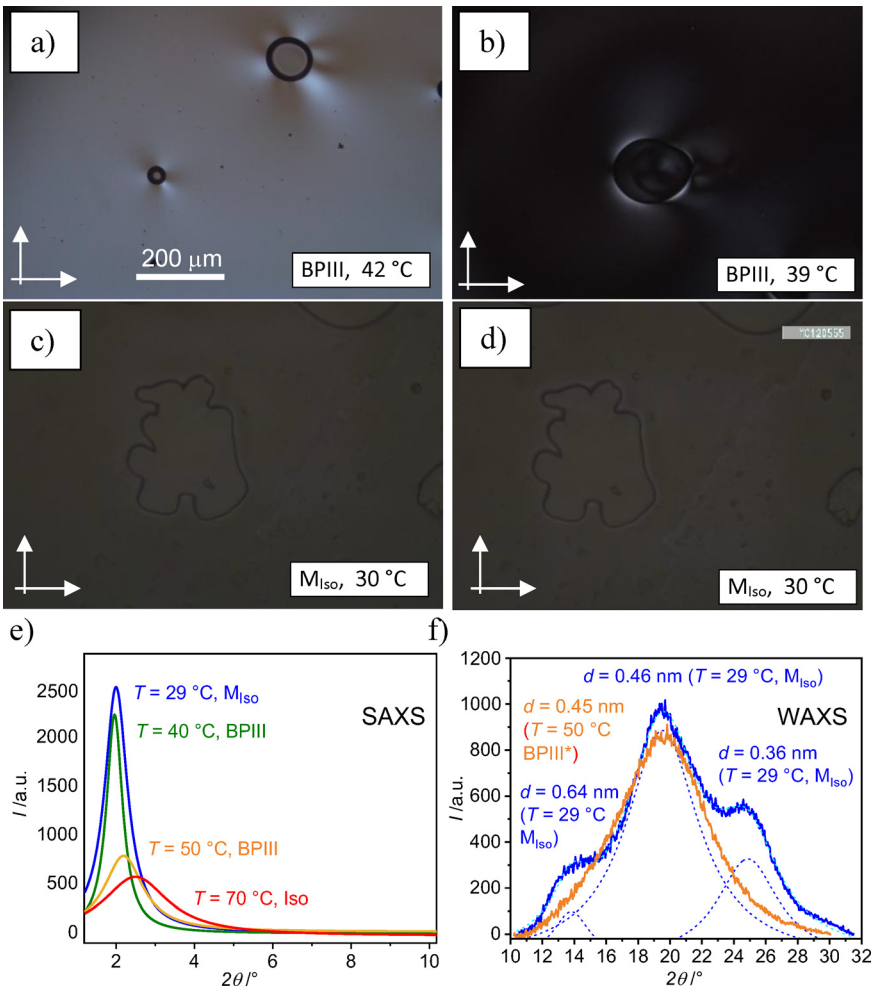

Fig. 5 Optical textures of **IIa** (with few air bubbles) as observed between ordinary glass plates under crossed polarizers (indicated by arrows) on cooling (scale bar refers to all textures); (a) and (b) BPIII phase (a) at T = 42 °C after cooling from the isotropic state, showing a faint bluish reflection color after shearing, and (b) at T = 39 °C; in both cases the sample is fluid; (c) texture of the M_{Iso} phase at 30 °C before and (d) after shearing, indicating that the sample is viscoelastic and no birefringence could be induced by shearing at this temperature; (e) Lorentz fits of the SAXS patterns (original patterns are shown in Fig. S52) and (f) WAXS patterns at the indicated temperatures; for more XRD data and correlation lengths, see Tables S2 and S3.

decrease of the correlation length L_ζ (from ~16 nm in BPIII) to ~12 nm, being almost the same value as found for the M_{Iso} phases of compounds **Ia-c** (L_ζ ~10–12 nm, see Table S2). Moreover, the WAXS pattern adopts the same typical shape with a maximum at 0.45 nm and shoulders at 0.36 and 0.64 nm as observed for compounds **Ia-c** (blue curve in Fig. 5(f)). Based on these results and the significant enthalpy associated with this phase transition, the optically isotropic low temperature mesophase of compound **IIa** is considered as the same M_{Iso} phase as found for compounds **Ia-c**. While heating, this M_{Iso} phase transforms directly into the isotropic liquid at 56 °C; its formation on cooling shows a significant hysteresis and obviously takes place in two steps with an intermediate amorphous blue phase (BPIII). It is considered as a helical cybotactic nematic phase with helix formation in all three spatial directions, but without organization of the resulting defects on a cubic 3D lattice. For bent-core compounds, the formation of such an amorphous BPIII phase was proposed to be supported by a competition between helical ordering and development of cybotactic SmC clusters, assuming heliconical twist (Fig. 2) in the chiral nematic phase.[101] The almost continuous formation of this chirality-modulated cybotactic nematic phase is in line with the apparent absence of a measurable enthalpy for the Iso–BPIII transition.

Overall, for **IIa** with only one branched chain, the driving forces for twist and curvature are smaller than in the double-branched series **I**. For this compound the transition to M_{Iso} takes place at a lower temperature and only after assuming local lamellar ordering (cybotaxis in BPIII) before face-to-face packing at the onset of layer formation leads to M_{Iso}. For the following homologues **IIb** and **IIc** with longer alkyl chains, the effects of chain branching and stereogenic centers on LC self-assembly become even weaker, and the highly frustrated isotropic M_{Iso} and BPIII phases are removed and replaced by less distorted birefringent mesophases.

3.2.2. Compound IIb with cholesteric N_{CybC}* and lamellar M_L* phases. Upon cooling, compound **IIb** exhibits a chiral nematic phase (cholesteric, N*) between 76 and 32 °C, as identified by a typical birefringent texture with oily streaks and a changing selective reflection color with temperature (Fig. 6(a), (c), (d) and Fig. S45). The XRD patterns feature a relatively broad SAXS with higher intensity than in Iso and a wide single WAXS around 0.45 nm, thus supporting a cybotactic type of N* phase (Fig. 6(k) and (l), orange curves).[62] The position of the SAXS indicates a periodicity of d = 4.6 nm in the cybotactic clusters and a longitudinal correlation length of L_ζ ~ 14 nm (3 molecules lengthwise) at 70 °C, which increases on cooling to L_ζ ~ 26 nm (5 molecules) at 50 °C, in line with growing cluster size (Table S2). Because the d-value is smaller than the molecular length (L_{mol} = 5.1 nm), it is concluded that the N* phase of **IIb** is composed of tilted smectic (SmC) clusters, and therefore designated as N_{CybC}*.[62] Its formation from the isotropic liquid is associated with a small DSC peak (ΔH ~ 0.6–0.8 kJ mol^{-1}, Fig. S44c) as typical for this kind of phase transition.[79]

The formation of the N_{CybC}* phase from Iso leads at 76 °C to a birefringent texture composed of Maltese crosses, indicating an arrangement of the helix axis parallel to the surfaces (Fig. 6(b) and 7(b)),[47,102] Upon further cooling from 76 and to 72 °C the texture slowly turns into an almost uniform texture with bluish selective reflection (Fig. 6(a) and (c)), indicating that the helix axis becomes aligned perpendicular to the surfaces (Fig. 7(a) and (c)).[47] This realignment of the helix is reversible and can be observed with inverted sequence upon heating at almost the same temperatures (Fig. S45). The same realignment is induced by shearing the initially formed focal conic texture (Fig. 6(b) → Fig. 6(a), (c)). Upon further cooling, the selective reflection is retained, and it is shifted from blue to green due to a widening of the helix pitch (Fig. 6(c) → Fig. 6(d)).

The transition to the low temperature phase at 42 °C, though having a large enthalpy (ΔH = 15.8 kJ mol^{-1}), is barely visible by POM, only indicated by a slightly darker appearance of the texture, though the birefringence as well as the selective reflection are retained (Fig. 6(d) → Fig. 6(e)). This means that, in contrast to **IIa**, the sample does not become optically isotropic at this transition (see areas around defects in Fig. 6(d) and (e)). At this temperature, the single diffuse WAXS in N_{CybC}* (Fig. 6(l), orange curve) splits into the same typical pattern with three maxima (Fig. 6(l), blue curve) as found for the M_{Iso} phases of compounds **Ia-c** and **IIa**, meaning that the low temperature phase should have fundamentally the same molecular organization (tilted face-to-face stacking in lamellae) as in the achiral isotropic M_{Iso} phase. However, as it remains birefringent, we designate this phase as M_L*, indicating a lamellar phase (L) with heliconical twist (*). The position of the SAXS does not change significantly from d = 4.6 to 4.7 nm at this transition (Fig. 6(k)), while the correlation length decreases from L_ζ ~ 26 nm in the N_{CybC}* phase at 50 °C to only L_ζ ~ 19 nm (4 molecules) in the M_L* phase at 35 °C (Table S2). This hints at a reduced size of the domains with uniformly organized molecules in M_L*, being even smaller than in the adjacent N_{CybC}* phase, due to the increasing layer distortion after assuming a denser face-to-face packing. However, as birefringence is retained (Fig. 6(e)), the degree of layer distortion in M_L* is reduced if compared with the isotropic M_{Iso} phases. This is in line with the increased correlation length of lamellar ordering of L_ζ ~ 19 nm for the M_L* phase of **IIb**, compared to only L_ζ ~ 11–12 nm in the M_{Iso} phases of compounds **I** (see Table S2).

It is also remarkable that only the brightness of the image decreases a bit, but no other change of the texture takes place at the N_{CybC}*–M_L* transition (Fig. 6(d) → Fig. 6(e)). This means that the alignment of the molecules between the surfaces, as well as the orientation of the helix axis, does not change at this transition, and that the layers/layer fragments should be aligned with their interfaces on average parallel to the surfaces in both mesophases, N_{CybC}* (Fig. 7(c)), and also in M_L*. From this observation, it can be concluded that in both mesophases the selective reflection is due to a heliconical twist of the molecules in and between the lamellar cluster (Fig. 7(c)), while in usual N* phases it is due to a helical twist of the individual molecules (Fig. 7(a)).[79]

In POM investigations of the M_L* phase at 29 °C (Fig. 6(f)–(j)), the rotation of the analyzer by +5° out of the 90° crossed

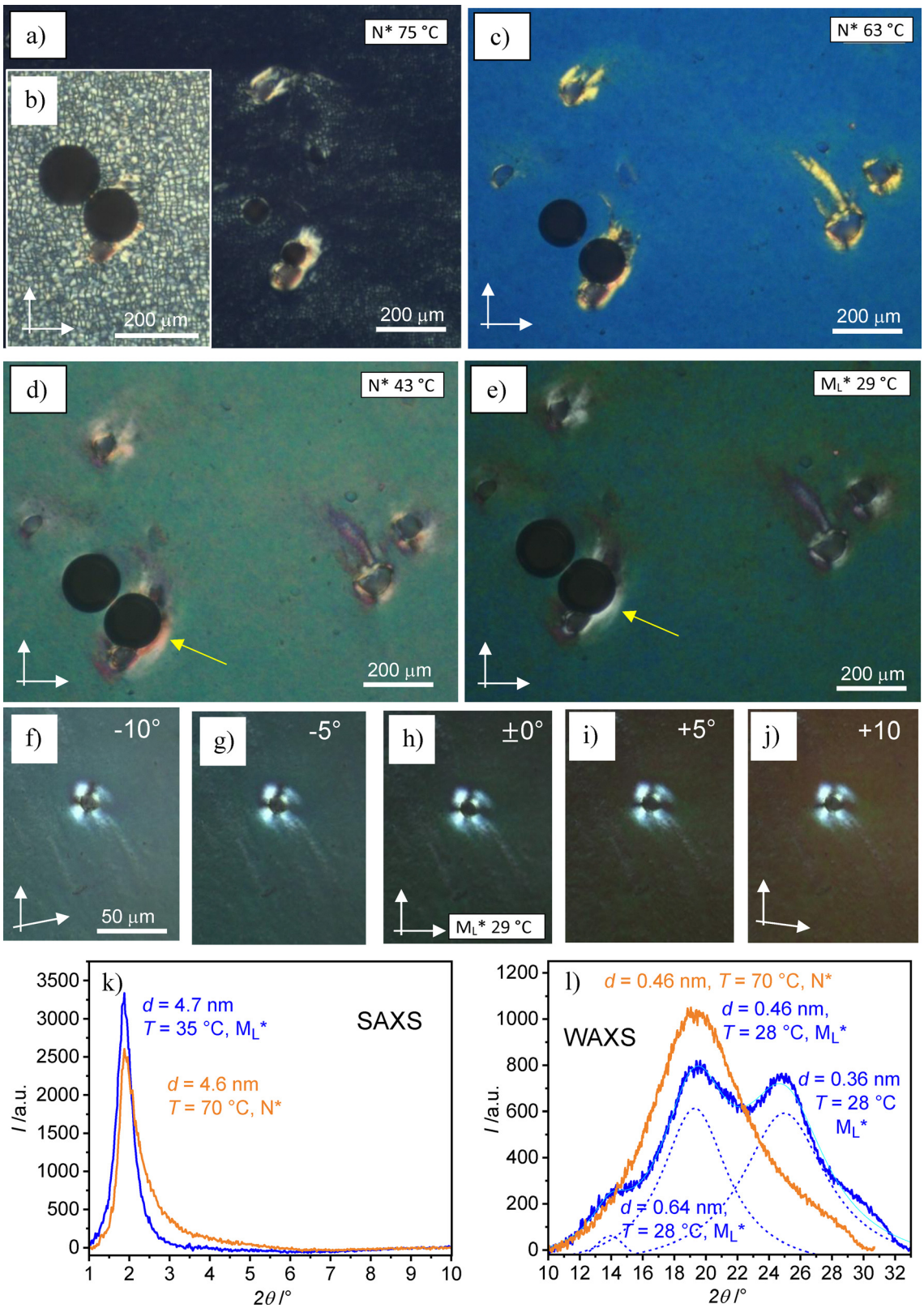

Fig. 6 Investigation of compound **IIb**. (a)–(e) POM textures (a), (c), (d) in the N_{CybC}* phase and (e) in the M_L* phase upon cooling between ordinary glass plates at identical illumination and exposure times; yellow arrows indicate areas of almost planar alignment around the defects; (b) shows the N_{CybC}* phase on heating just before the transition to Iso, the same texture is found on cooling from Iso, while textures (a) was obtained after shearing the sample; the dark circles are air bubbles; birefringence is mainly observed around these defects while the color in the dominating areas stems from selective refection. (f)–(j) Textures of the M_L* phase as observed at 29 °C by POM and rotating the analyzer by the given angles out of the 90° orientation, maximum darkness is achieved at +5°, indicating the presence of optical rotation. Rotating the sample between crossed polarizers leads to no change, confirming homeotropic alignment; (k) SAXS and (l) WAXS patterns in the N_{CybC}* and M_L* phases at the indicated temperatures; for more X-ray data and correlation lengths, see Tables S2 and S3.

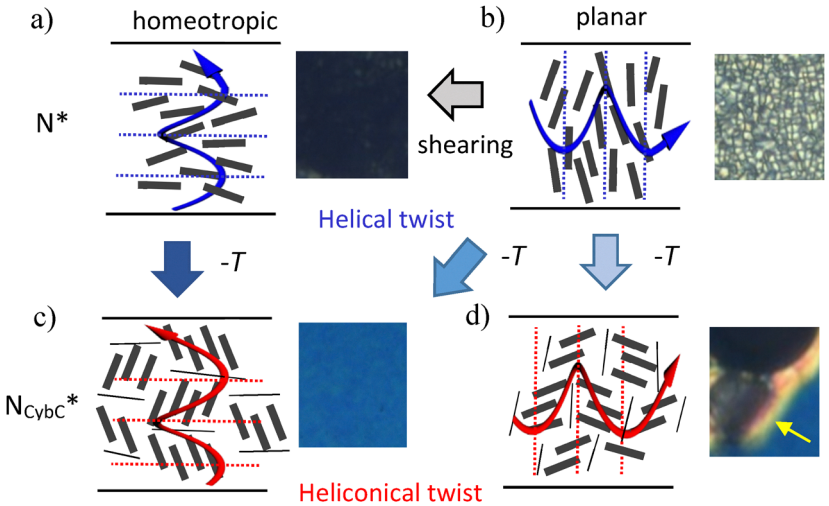

Fig. 7 Schematics of (a) and (b) helical (blue helix) and (c) and (d) heliconical (red helix) chiral nematic phases with typical textures. Realignment of molecular and helical direction at the transition from the almost "molecular" helical cholesterics at high temperature to heliconical cybotactic N_{CybC}*-type cholesteric LC phases by growth of the cybotactic SmC* clusters at lowering temperature (though the molecules are actually bent, they are simplified as rods, also the helical twist of the individual molecules is for simplicity not shown in perspective view); the dotted lines indicate the orientation of the periodicity resulting from identical molecular orientation along the helix axis, and correspond to half the helical pitch; homeotropic and planar refer to the orientation of these planes with respect to the substrate surfaces, as shown; a birefringent texture (b) and (d) is observed between crossed polarizers for the cholesteric phases if these layers are aligned perpendicular to the substrate surfaces, alignment parallel to the surfaces gives an pseudo-isotropic textures with or without selective reflection color (a) and (c).

orientation with respect to the polarizer (Fig. 6(i)) leads to maximal darkness, confirming the uniform chirality of this phase. Thus, the M_L* phase has a heliconical SmC*-like structure with restricted rotation of the molecules around their long axis and preferred face-to-face packing (SmC_b, Fig. 3(f)), though the layers are less distorted than in the M_{Iso} phase. In the almost flat layers, the heliconical twist is retained and dominates over the helical. The thus reduced helical twist decreases the layer distortion, increases correlation length, and thus retains birefringence. The reduced layer distortion is due to the lower density of chain branching, respectively, stereogenic centers in the singly branched compound **IIb** compared to compounds **Ia-c** and to compound **IIa** with shorter chains.

3.2.3. Compound IIc with N_{CybC}*–SmC*–M_L* sequence. Compound **IIc** shows three DSC peaks upon heating (Fig. 4(b)). On cooling from the isotropic liquid, firstly, the focal conic texture of the N_{CybC}* phase is observed below 86 °C (1.0–1.3 kJ mol^{-1}), which upon shearing or with decreasing temperature becomes a typical oily streaks texture with deep blue selective reflection color (Fig. 8(a)), very similar to the N_{CybC}* phase of **IIb**. On further cooling, the reflection color changes to green, indicating an expansion of the helix pitch (Fig. 8(b)). As described for **IIb**, the helix axis is perpendicular to the layers in the cybotactic clusters, *i.e.*, the twist is heliconical (Fig. 7(c)). As is typical for N_{CybC}* phases, the SAXS is relatively broad and more intense than in Iso (Fig. 8(g)), and the correlation length increases with lowering temperature due to the growing cluster size.

At the transition with very small enthalpy (0.1 kJ mol^{-1}, Fig. 4(b)) at 74 °C, the texture undergoes a pronounced color change of the selective reflection color to faint bluish (Fig. 8(c)). Simultaneously, the SAXS suddenly becomes sharp at this transition (Fig. 8(g), green curve) while the WAXS does not change (Fig. 8(h), green curve), indicating the transition to a non-distorted fluid smectic phase. The layer spacing d = 4.1–4.2 nm is in line with a tilted organization of the molecules (L_{mol} = 5.7 nm), while the presence of a selective reflection in homeotropic alignment and the rotation of the plane of polarized light (Fig. S47) indicates heliconical twist and uniform phase chirality; thus, this phase is assigned as SmC*. The correlation length is about $L_\zeta \sim 56$ nm, corresponding to 10–12 molecular lengths at 60 °C, which means that there are almost no layer distortions in the SmC* phase, but nevertheless, no ferroelectric switching can be observed, probably due to residual layer modulation.

On further cooling, the bluish reflection color first intensifies and then turns into green (Fig. 8(d) and (e)), and the SAXS scattering becomes broader already in the SmC* range, even before the next phase transition (see Fig. 8(g), dashed green curve). The correlation length decreases from $L_\zeta \sim 56$ nm at 60 °C to $L_\zeta \sim 30$ nm at 50 °C, corresponding to only 6 molecular lengths (see Table S2), while the WAXS remains diffused, showing only a single broad scattering (Fig. 8(h), green curve). The next phase transition with high enthalpy (16 kJ mol^{-1}, Fig. 4(b)) at 42 °C (upon cooling) is optically only indicated by a slight change of the selective reflection color from greenish to bluish (Fig. 8(e) → Fig. 8(f)) while the phase remains birefringent though the birefringence decreases at this transition as also observed for **IIb** (see planar areas around the defects, Fig. 8(e) and (f)). In the X-ray diffraction pattern, there is a further broadening of the SAXS ($L_\zeta \sim 20$ nm ~ 4 molecules at T = 35 °C, Table S1) and the emergence of the typical triple

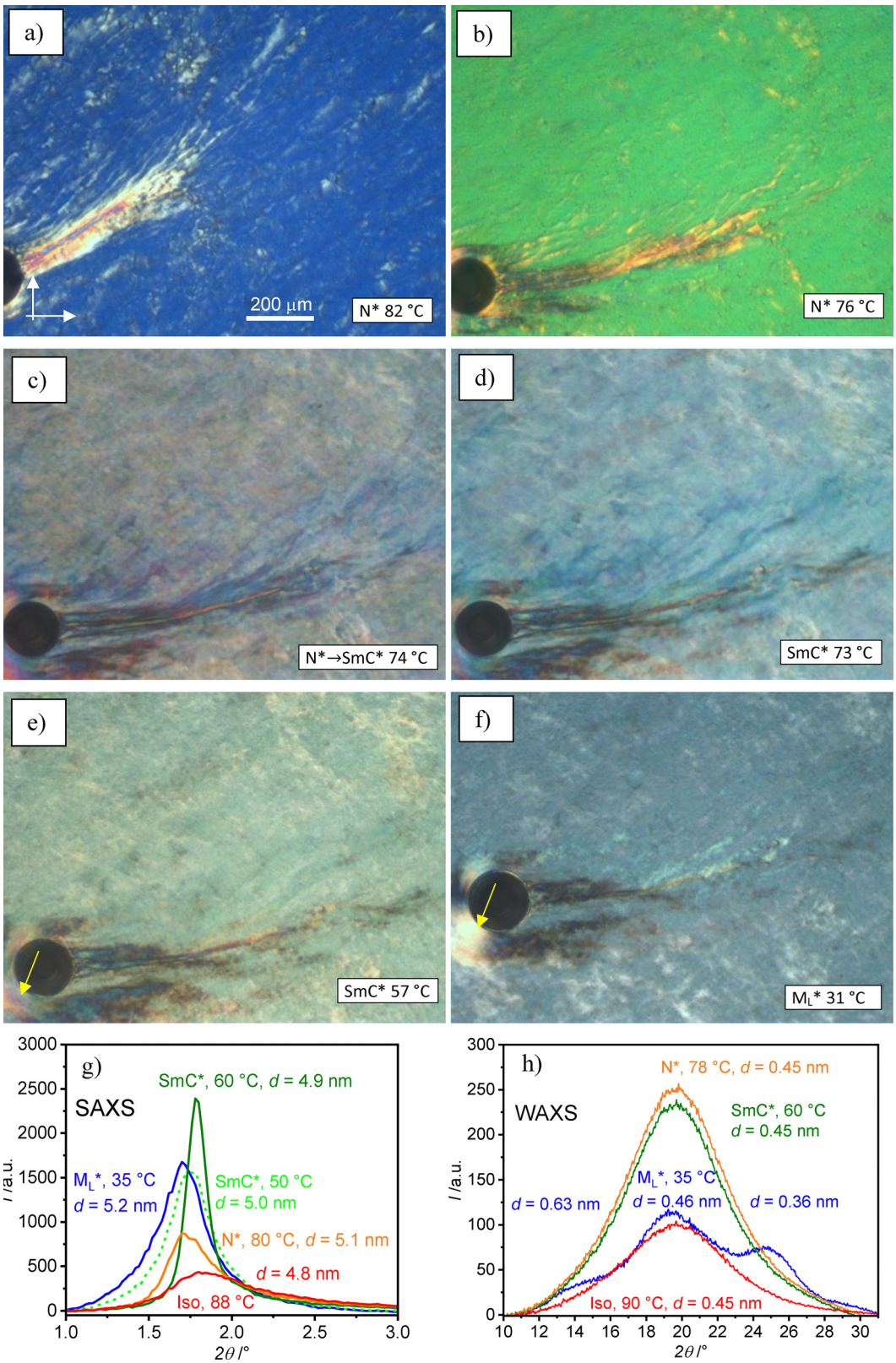

Fig. 8 (a)–(f) Optical textures of bent-core molecule **IIc** as observed on cooling between ordinary glass plates under crossed polarizers (indicated by arrows) and after shearing the sample, recorded at identical illumination and exposure time at the given temperatures (scale bars refer to all textues); (g) SAXS and (h) WAXS patterns at the indicated temperatures.

maxima pattern of the M_L* phase in the WAXS (Fig. 8(g), (h), blue curves). This is in line with the increasing layer distortion after restriction of the molecular rotation at the SmC* → M_L* transition. Compared to **IIb**, chain elongation leads to an additional almost non-distorted SmC* range occurring between the cybotactic nematic and the M_L* phase.

3.3. Overall phase sequence

The full sequence of LC phases formed by compounds **I** and **II**, depending on temperature and density of chain branching, is shown in Fig. 9. The layer distorting force decreases from series **I** with two branched chains, forming the isotropic M_{Iso} phase, to series **II** with only one branching. In series **II**, it decreases with chain elongation from **IIa** to **IIc**, thus compound **IIa** with the shortest chains represents an intermediate case showing the same M_{Iso} phase as found in series **I**, but in this case, accompanied by BPIII. Elongation of the chains further reduces the layer distortion and provides a less distorted M_L* phase. While in series **I**, the M_{Iso} phase is directly formed from the isotropic liquid on cooling, the M_{Iso} and M_L* phases of series **II** are accompanied by additional LC phases involving heliconical twist. In both series, layer distortion arises with the emergence of restricted molecular rotation by face-to-face stacking of the polyaromatic cores, leading to a denser core packing and emerging short-range in-plane ordering, which obviously increases the driving force for saddle-splay deformation. The strength of distortion also increases with the density of the chiral chain-branching points. However, we cannot decide if the main contribution to layer distortion comes from the steric constraints implied by the chain branching or from the helical twisting power (HTP) of the stereogenic centers, which would require comparison with the corresponding racemic compounds **I** and **II**; this will be the focus of future work.

3.4. Chiral self-assembly in the isotropic mesophase (M_{Iso})

The M_{Iso} and M_L* phases are considered as distorted versions of the tilted lamellar phases with restricted rotation due to face-to-face packing. Thus, they can be considered as structures located between liquid crystalline and soft crystalline self-assembly, similar to the hexatic phases being located between the fluid LC phases (SmA, SmC) and the soft crystalline mesophases. While the previously reported isotropic mesophases of bent-core mesogens show ambidextrous mirror symmetry breaking for achiral molecules, which is affected by permanent molecular chirality (and then often leading to uniform chirality[50,51,53]), the compounds reported here are

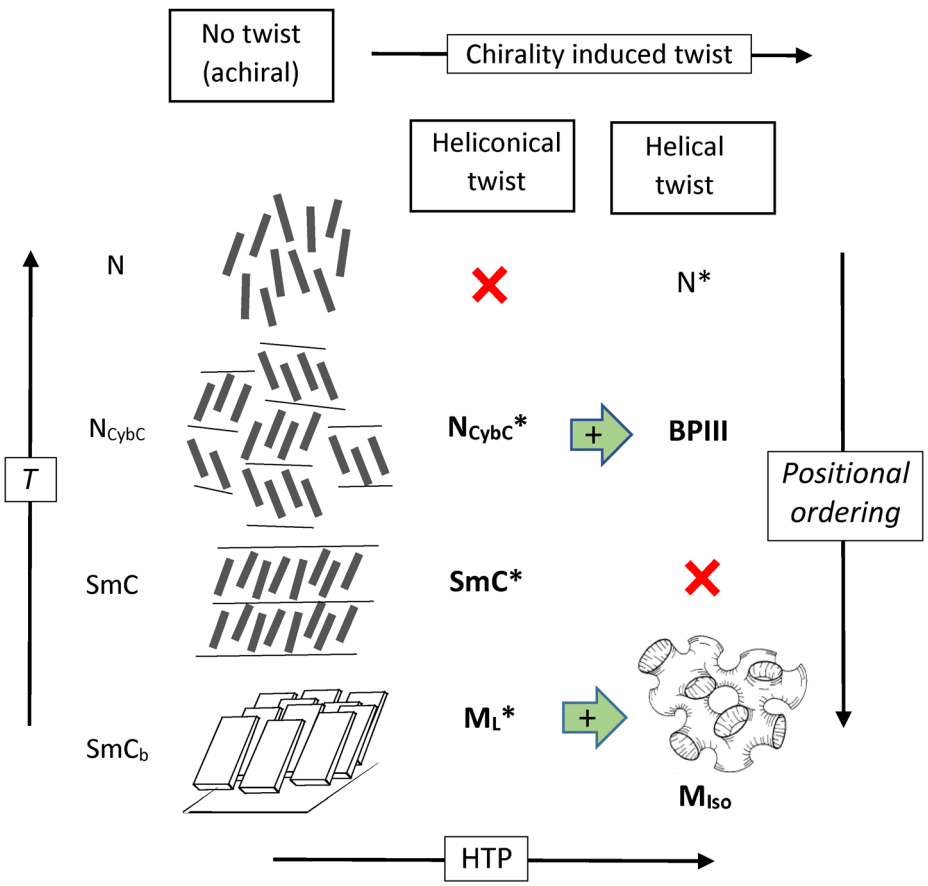

Fig. 9 Development of heliconical and helical twist (Fig. 2) in the LC phases of compounds **I** and **II** with growing lamellar ordering and helical twisting power (HTP); the green arrows indicate the combination of heliconical and helical twist; the bent-shaped molecules are simplified and shown as rods resulting from the rotational disorder around the long axes or as boards for restricted rotation with face-to-face stacking, but without polar order.

permanently chiral in all cases. While uniform chirality is observed in M_L*, the unique feature of the M_{Iso} phase is the absence of recognizable superstructural chirality despite the molecular chirality. Because the density of chiral branching increases from M_L* to M_{Iso} it is likely that the M_{Iso} phase represents the more strongly frustrated phase, most probably combining saddle splay with helical twist of the polyaromatic cores. Because it is known that the mode of helix interaction depends on the pitch length and the spatial orientation of the helices,[103–106] it is possible that the preferred helix–helix interaction could change from enantiophobic (preferring uniform helicity) in M_L* to enantiophilic (preferring opposite helicity) in M_{Iso}, the latter case intrinsically supporting a racemic phase structure.[103] This is, for example, known for the double gyroid phase,[103,107] an achiral bicontinuous cubic mesophase composed of two enantiomorphic helical networks separated by a minimal surface based on a saddle splay curved layer.[44] It might be considered as a long-range ordered version of the sponge-like structure in M_{Iso}. However, then the question arises, why is the molecular chirality incapable of breaking the mirror symmetry of this racemic superstructure? Here, it needs to be considered that chain branching and the *gauche* effect of the –OCH_2–$CH(CH_3)$O-linkage support non-linear conformations, thus providing significant flexibility of the linkage between polyaromatic core and the stereogenic centers, allowing different orientations of the stereogenic center(s) with respect to the local helicity of the organization of the polyaromatic cores. This decoupling between superstructural and molecular chirality might reduce the effects of the molecular chirality to such an extent that it cannot overcome the enantiophilic mode of interhelical packing in M_{Iso}, similar to some previously reported cases of bicontinuous cubic LC phases.[53,58]

3.5. Related isotropic mesophases of rod-like molecules

As noted above, isotropic mesophases are quite common for bent-core mesogens (DC, HNF), but interestingly, there are also a few reports about non-cubic isotropic mesophases of rod-like molecules. Only recently re-entrant isotropic mesophases (I_{re}) occurring below heliconical LC phases, either a SmC* (W470)[108] or a ferroelectric nematic phase (N_F) phase (RM734,[109] DIO[110]),[111] were found for the mentioned linear molecules; for chemical structures, see Fig. S55. The common feature of the M_{Iso} phases reported here and the I_{re} phases is a WAXS composed of at least three diffuse maxima located at 0.57, 0.45 nm, and around 0.37 nm for W470[108] and around 0.70, 0.45, and 0.37 nm for DIO (Fig. S56).[112] However, in these I_{re}-phases, the SAXS scatterings are a bit sharper than those found for M_{Iso}, and there are additional sharp SAXS reflections (see Fig. S55). This means that the M_{Iso} phase apparently has a reduced correlation length of in-plane order compared to these I_{re} phases, and these I_{re} phases are a bit more crystal-like. This is presumably due to the additional contribution of the layer deformation by the intrinsic saddle splay curvature induced by the bent molecular shape (Fig. 1 and 2) and being absent for the rod-like compounds. Nevertheless, it is remarkable that achiral isotropic mesophases can be observed in very different classes of mesogens, ranging from chirality frustrated rods (W470) *via* polar ordered rods (RM734 and DIO) to bent-core molecules (**Ia-c**, **IIa**). All these isotropic mesophases appear to be somehow related to the emergence of helical/heliconical twist.

4. Conclusions

Two series of 4-cyanoresorcinol based bent-core molecules carrying a chiral (*S*)-2-alkyloxypropyl end group at both or only one end (Scheme 2) have been synthesized and the effects of the number of chain-branching and chain length on LC self-assembly were investigated (Fig. 9). Two new mesophases with tilted molecules, restricted rotation around the long axis, preferred face-to-face stacking of the polyaromatic cores and only short correlation length of lamellar ordering were discovered. One is apparently achiral and isotropic (M_{Iso}) while the other one is chiral and low birefringent (M_L*). Which of them is formed depends on the number of branched chains and their length. With increasing concentration of the branching points, the layer distortion increases, and the birefringent heliconical M_L* phase is replaced by the achiral isotropic M_{Iso} phase. For the latter, a combination of saddle-splay and helical twist is considered as responsible for the layer distortion and formation of this sponge-like phase. Having restricted molecular rotation and some in-plane order, both M phases represent intermediate cases bridging the gap between the isotropic LC phases with sponge-like deformed fluid layers[14,22,33] and the HNF phases formed by crystallized helical filaments.[18,38]

For compounds **II** with only one branched chain, additional mesophases occur at temperatures above the M phases, namely an amorphous (type III) blue phase (**IIa**), a heliconical SmC* phase, and a chiral cybotactic nematic phase composed of SmC* clusters (N_{CybC}*). It is shown that in the cybotactic N_{CybC}* phase of compounds **IIb,c**, and most likely also for the chiral cybotactic nematic phases of other (bent-core) mesogens,[78,79] the twist is heliconical instead of helical as usually found for non-cybotactic cholesteric phases of most rod-like molecules (Fig. 2). As the helical twist is hindered by the developing lamellar organization, the transition from helical to heliconical twist takes place as the size of the cybotactic clusters grows upon lowering temperature (Fig. 7(b) and Fig. 7(c)). This means that cybotactic cluster formation changes the chiral nematic phase from helical to heliconical (Fig. 7). This observation not only allows the selection and switching of the helical twist direction, but it also suggests that cybotaxis is likely to contribute to the development of the heliconical twist in other soft matter systems, as, for example, in the BPIII phases of chiral bent-core mesogens and the recently discovered twist-bend nematic (N_{TB})[28] and ferroelectric nematic (N_F, N_F^{hel}) phases of achiral compounds.[30,113]

The BPIII-like phase, characterized by twist in all three spatial directions, is considered as an organization of cybotactic clusters that combine both helical and heliconical twist. In this regard, it shares similarities with the M_{Iso} phase but lacks restricted rotation around the molecular long axis. The

potential for BPIII phase formation through the coupling of heliconical and helical twist is particularly noteworthy. These isotropic mesophases are rarely observed and exhibit rapid response times to an electric field, do not require an alignment layer, and show no birefringence at zero voltage.[93] These properties highlight their significant application potential in fast-switching light modulators and displays.

In conclusion, the 4-cyanoresorcinol-based bent-core liquid crystals (BCLCs) represent a valuable class of compounds for investigating complex LC self-assembly and discovering novel phase structures. This research provides critical insights into the relationships between molecular structure, mesophase formation, and properties for the design of new LC materials for potential technological applications.

Author contributions

H. O. G. and M. A. conceived the concept, supervised the project, provided funding, were responsible for project administration, wrote the first draft, and revised the manuscript. C. T. conceived the concept, co-supervised the project, revised the manuscript, and performed additional optical characterization. B. Y. Ö. and A. Ö. performed the synthesis and investigations. C. A. performed the XRD investigations. D. K. B. co-supervised the project.

Conflicts of interest

There are no conflicts to declare.

Data availability

The data supporting this article have been included as part of the supplementary information (SI). Supplementary information is available. See DOI: https://doi.org/10.1039/d5tc03348a.

Acknowledgements

This work was supported by TUBITAK International Cooperation Projects Research Support Group in the framework of the Protocol on Cooperation in Science and Technology between The Scientific and Technological Research Council of Türkiye (TUBITAK), the German Academic Exchange Service (DAAD) with the project number: 221N431 and the Deutsche Forschungsgemeinschaft (DFG, no. AL2378/1-2, 424355983, 436494874 – GRK 2670). H. O. G. is also grateful to the Alexander von Humboldt Foundation for a research fellowship at Martin Luther University, Halle, Germany.

References

1 *Handbook of Liquid Crystals*, ed. J. W. Goodby, P. J. Collings, T. Kato, C. Tschierske, H. Gleeson and P. Raynes, Wiley-VCH, Weinheim, 2014.
2 P. J. Collings and M. Hird, *Introduction to Liquid Crystals: Chemistry and Physics*, Taylor & Francis, CRC Press, London, 1997.
3 C. Tschierske, *Angew. Chem., Int. Ed.*, 2013, **52**, 8828–8878.
4 H. K. Bisoyi and Q. Li, *Chem. Rev.*, 2022, **122**, 4887–4926.
5 J. Uchida, B. Soberats, M. Gupta and T. Kato, *Adv. Mater.*, 2022, **34**, 2109063.
6 C. Esteves, E. Ramou, A. R. P. Porteira, A. J. M. Barbosa and A. C. A. Roque, *Adv. Opt. Mater.*, 2020, **8**, 1902117.
7 S. Sergeyev, W. Pisula and Y. H. Geerts, *Chem. Soc. Rev.*, 2007, **36**, 1902–1929.
8 H. K. Bisoyi and Q. Li, *Prog. Mater. Sci.*, 2019, **104**, 1–52.
9 E.-K. Fleischmann and R. Zentel, *Angew. Chem., Int. Ed.*, 2013, **52**, 8810.
10 T. Kato, J. Uchida, T. Ichikawa and T. Sakamoto, *Angew. Chem., Int. Ed.*, 2018, **57**, 4355–4371.
11 (*a*) C. Tschierske, *Isr. J. Chem.*, 2012, **52**, 935–959; (*b*) Y. Cao, Y. Zhao, T. Tan, F. Liu and M. Alaasar, *Chem. – Eur. J.*, 2025, **31**, e202403586.
12 T. Niori, T. Sekine, J. Watanabe, T. Furukawa and H. Takezoe, *J. Mater. Chem.*, 1996, **6**, 1231–1233.
13 G. Pelzl, S. Diele and W. Weissflog, *Adv. Mater.*, 1999, **11**, 707–724.
14 R. A. Reddy and C. Tschierske, *J. Mater. Chem.*, 2006, **16**, 907–961.
15 H. Takezoe and A. Eremin, *Bent-Shaped Liquid Crystals*, Taylor and Francis, Boca Raton, FL, 2017.
16 M. Alaasar, *Liq. Cryst.*, 2016, **43**, 2208–2243.
17 S. Kaur, V. Punjani, N. Yadav, A. Barthakur, A. Baghla, S. Dhara and S. K. Pal, *Liq. Cryst.*, 2022, **49**, 1078–1146.
18 H. Takezoe, *Top. Curr. Chem.*, 2011, **318**, 303–330.
19 C. Tschierske, *Liq. Cryst.*, 2018, **45**, 2221–2252.
20 A. Yoshizawa, *Crystals*, 2024, **14**, 97.
21 D. R. Link, G. Natale, R. Shao, J. E. Maclennan, E. Körblova, N. A. Clark and D. M. Walba, *Science*, 1997, **278**, 1924–1927.
22 L. E. Hough, M. Spannuth, M. Nakata, D. A. Coleman, C. D. Jones, G. Dantlgraber, C. Tschierske, J. Watanabe, E. Körblova, D. M. Walba, J. E. Maclennan, M. A. Glaser and N. A. Clark, *Science*, 2009, **325**, 452–456.
23 T. Sekine, T. Niori, J. Watanabe, S. W. Choi, Y. Takanishi and H. Takezoe, *J. Mater. Chem.*, 1997, **7**, 1307–1309.
24 This spontaneous superstructural chirality could be caused by the intrinsic ''layer chirality'' due to the orthogonal combination of polar order, tilt direction, and layer normal.[21] However, as there is no indication of polar order in the investigated systems, we disregard this possibility.
25 C. Tschierske and G. Ungar, *ChemPhysChem*, 2016, **17**, 9–26.
26 *Chirality in Liquid Crystals*, ed. H. S. Kitzerow and C. Bahr, Springer, New York, 2001.
27 V. Borshch, Y. K. Kim, J. Xiang, M. Gao, A. Jakli, V. P. Panov, J. K. Vij, C. T. Imrie, M. G. Tamba, G. H. Mehl and O. D. Lavrentovich, *Nat. Commun.*, 2013, **4**, 2635.
28 R. J. Mandle, *Molecules*, 2022, **27**, 2689.
29 A. F. Alshammari, A. Zattarina, A. Pearson, E. Cruickshank, M. Majewska, D. Pociecha, J. M. D. Storey, E. Gorecka, C. T. Imrie and R. Walker, *Liq. Cryst.*, 2024, **51**, 2300–2312.

30 Y. Song, S. Aya and M. Huang, *Giant*, 2024, **19**, 100318.
31 G. Porte, J. Appell, P. Bassereau, J. Marignan, M. Skouri, I. Billard and M. Delsanti, *Phys. A*, 1996, **176**, 168–186.
32 J. Thisayukta, Y. Nakayama, S. Kawauchi, H. Takezoe and J. Watanabe, *J. Am. Chem. Soc.*, 2000, **122**, 7441–7448.
33 G. Dantlgraber, A. Eremin, S. Diele, A. Hauser, H. Kresse, G. Pelzl and C. Tschierske, *Angew. Chem., Int. Ed.*, 2002, **41**, 2408–2412.
34 M. Nagaraj, *Liq. Cryst.*, 2016, **43**, 2244–2253.
35 R. S. Hegde, J. Kumar and V. Prasad, *Liq. Cryst.*, 2019, **46**, 1091–1107.
36 O. Bazavan, S. K. Saha, M. K. Paul and I. Dierking, *J. Mol. Liq.*, 2020, **315**, 113706.
37 D. Chen, H. Wang, M. Li, M. A. Glaser, J. E. Maclennan and N. A. Clark, *Soft Matter*, 2014, **10**, 9105–9109.
38 L. E. Hough, H. T. Jung, D. Kruerke, M. S. Haeberling, M. Nakata, C. D. Jones, D. Chen, D. R. Link, J. Zasadzinski, G. Heppke, J. P. Rabe, W. Stocker, E. Körblova, D. M. Walba, M. A. Glaser and N. A. Clark, *Science*, 2009, **325**, 456–460.
39 K. V. Le and H. Takezoe, *Adv. Mater.*, 2017, **29**, 1602737.
40 A. Gowda, G. Acharjee, S. K. Pathak, G. A. R. Rohaley, A. Shah, R. P. Lemieux, M. E. Prevot and T. Hegmann, *Mater. Horiz.*, 2024, **11**, 5550–5563.
41 J. Liu, S. Shadpour, M. E. Prévôt, M. Chirgwin, A. Nemati, E. Hegmann, R. P. Lemieux and T. Hegmann, *ACS Nano*, 2021, **15**, 7249–7270.
42 M. Alaasar, M. Prehm and C. Tschierske, *Chem. – Eur. J.*, 2016, **22**, 6583–6597.
43 K. V. Le, M. R. Tuchband, H. Iwayama, Y. Takanishi, N. A. Clark and F. Araoka, *arXiv*, 2022, arXiv:2210.13544.
44 D. Chen, Y. Shen, J. Aguero, E. Korblova, D. M. Walba, N. Kapernaum, F. Giesselmann, J. Watanabe, J. E. Maclennan, M. A. Glaser and N. A. Clark, *ChemPhysChem*, 2014, **15**, 1502–1507.
45 J.-J. Lee, S. Kim, H. Nishikawa, Y. Takanishi, H. Iwayama, C. Kim, S.-W. Choi and F. Araoka, *Int. J. Mol. Sci.*, 2022, **23**, 14629.
46 I. Dierking, *Symmetry*, 2014, **6**, 444–472.
47 D. S. Kumari, C. Anders, M. Alaasar, V. Jayalakshmi and G. Shanker, *Liq. Cryst.*, 2025, DOI: **10.1080/02678292.2025.2539166**.
48 R. A. Reddy, B. K. Sadashiva and U. Baumeister, *J. Mater. Chem.*, 2005, **15**, 3303–3316.
49 C. V. Yelamaggad, I. S. Shashikala, G. Liao, D. S. Shankar Rao, S. K. Prasad and Q. Li, *Chem. Mater.*, 2006, **18**, 6100–6102.
50 H. Ocak, B. Bilgin-Eran, M. Prehm and C. Tschierske, *Soft Matter*, 2012, **8**, 7773–7783.
51 H. Ocak, B. Bilgin-Eran, M. Prehm and C. Tschierske, *Soft Matter*, 2013, **9**, 4590–4597.
52 S. Anjali and R. Pratibha, *RSC Adv.*, 2016, **6**, 53830–53838.
53 A. Baghla, V. Punjani, D. S. Shankar Rao, S. K. Prasad and S. K. Pal, *J. Mater. Chem. C*, 2024, **12**, 3915–3923.
54 D. Chen, M. R. Tuchband, B. Horanyi, E. Korblova, D. M. Walba, M. A. Glaser, J. E. Maclennan and N. A. Clark, *Nat. Commun.*, 2015, **6**, 7763.
55 A. Gowda, S. K. Pathak, G. A. R. Rohaley, G. Acharjee, A. Oprandi, R. Williams, M. E. Prevot and T. Hegmann, *Mater. Horiz.*, 2024, **11**, 316–340.
56 S. Shadpour, A. Nemati, M. Salamonczyk, M. E. Prévôt, J. Liu, N. J. Boyd, M. R. Wilson, C. Zhu, E. Hegmann, A. I. Jákli and T. Hegmann, *Small*, 2020, **16**, 1905591.
57 S.-C. Lin, R.-M. Ho, C.-Y. Chang and C.-S. Hsu, *Chem. – Eur. J.*, 2012, **18**, 9091–9098.
58 M. Nakata, D. R. Link, F. Araoka, J. Thisayukta, Y. Takanishi, K. Ishikawa, J. Watanabe and H. Takezoe, *Liq. Cryst.*, 2001, **28**, 1301–1308.
59 I. Wirth, S. Diele, A. Eremin, G. Pelzl, S. Grande, L. Kovalenko, N. Pancenko and W. Weissflog, *J. Mater. Chem.*, 2001, **11**, 1642–1650.
60 L. Kovalenko, M. W. Schröder, R. A. Reddy, S. Diele, G. Pelzl and W. Weissflog, *Liq. Cryst.*, 2005, **32**, 857–865.
61 (*a*) C. Tschierske, *Liq. Cryst.*, 2022, **49**, 1043–1077; (*b*) M. Alaasar, S. Poppe and C. Tschierske, *Liq. Cryst.*, 2017, **44**, 729–737; (*c*) M. Alaasar, M. Prehm and C. Tschierske, *Liq. Cryst.*, 2014, **41**, 126–136.
62 C. Keith, A. Lehmann, U. Baumeister, M. Prehm and C. Tschierske, *Soft Matter*, 2010, **6**, 1704–1721.
63 (*a*) Y. Jang, R. Balachandran, C. Keith, A. Lehmann, C. Tschierske and J. K. Vij, *Soft Matter*, 2012, **8**, 10479–10485; (*b*) P. S. Salter, P. W. Benzie, R. A. Reddy, C. Tschierske, S. J. Elston and E. P. Raynes, *Phys. Rev. E: Stat., Nonlinear, Soft Matter Phys.*, 2009, **80**, 031701.
64 M. Alaasar, M. Prehm, M. Nagaraj, J. K. Vij and C. Tschierske, *Adv. Mater.*, 2013, **25**, 2186–2191.
65 A. Eremin, S. Diele, G. Pelzl, H. Nádasi, W. Weissflog, J. Salfetnikova and H. Kresse, *Phys. Rev. E: Stat., Nonlinear, Soft Matter Phys.*, 2001, **64**, 051707.
66 C. Keith, M. Prehm and C. Tschierske, *Chem. Commun.*, 2010, **46**, 3702–3704.
67 G. Shanker, M. Prehm, M. Nagaraj, J. K. Vij and C. Tschierske, *J. Mater. Chem.*, 2011, **21**, 18711–18714.
68 S. P. Sreenilayam, Y. P. Panarin, J. K. Vij, V. P. Panov, A. Lehmann, M. Poppe, M. Prehm and C. Tschierske, *Nat. Commun.*, 2016, **7**, 11369.
69 A. A. S. Green, M. R. Tuchband, R. Shao, Y. Shen, R. Visvanathan, A. E. Duncan, A. Lehmann, C. Tschierske, E. D. Carlson, E. Guzman, M. Kolber, D. M. Walba, C. S. Park, M. A. Glaser, J. E. Maclennan and N. A. Clark, *Phys. Rev. Lett.*, 2019, **122**, 107801.
70 A. Lehmann, M. Alaasar, M. Poppe, S. Poppe, M. Prehm, M. Nagaraj, S. P. Sreenilayam, Y. P. Panarin, J. K. Vij and C. Tschierske, *Chem. – Eur. J.*, 2020, **26**, 4714–4733.
71 M. Alaasar, M. Prehm, M.-G. Tamba, N. Sebastian, A. Eremin, Y. P. Panarin, J. K. Vij and C. Tschierske, *J. Mater. Chem. C*, 2025, **13**, 12513–12532.
72 N. Sebastian, S. Belau, A. Eremin, M. Alaasar, M. Prehm and C. Tschierske, *Phys. Chem. Chem. Phys.*, 2017, **19**, 5895–5905.
73 M. Alaasar, M. Prehm, S. Poppe and C. Tschierske, *Chem. – Eur. J.*, 2017, **23**, 5541–5556.

74 M. Alaasar, M. Prehm, S. Belau, N. Sebastián, M. Kurachkina, A. Eremin, C. Chen, F. Liu and C. Tschierske, *Chem. – Eur. J.*, 2019, **25**, 6362.
75 M. Alaasar, M. Prehm, K. May, A. Eremin and C. Tschierske, *Adv. Funct. Mater.*, 2014, **24**, 1703–1717.
76 V. Punjani, G. Mohiuddin, S. Kaur, A. R. Choudhury, S. Paladugu, S. Dhara, S. Ghosh and S. K. Pal, *Chem. – Eur. J.*, 2020, **26**, 5859–5871.
77 H. Ocak, M. Poppe, B. Bilgin-Eran, G. Karanlık, M. Prehm and C. Tschierske, *Soft Matter*, 2016, **12**, 7405–7422.
78 H. Ocak, B. Bilgin-Eran, M. Prehm, S. Schymura, J. P. F. Lagerwall and C. Tschierske, *Soft Matter*, 2011, **7**, 8266–8280.
79 H. Ocak, B. Bilgin-Eran, N. Nuray, A. Özkonstanyan, S. Poppe and C. Tschierske, *J. Mater. Chem. C*, 2021, **9**, 1895–1910.
80 H. Ocak, B. Bilgin-Eran, D. Güzeller, M. Prehm and C. Tschierske, *Chem. Commun.*, 2015, **51**, 7512–7515.
81 C. Tschierske, D. Joachimi, H. Zaschke, H. Kresse, B. Linström, G. Pelzl and D. Demus, *Mol. Cryst. Liq. Cryst.*, 1990, **191**, 231–236.
82 B. Barman, B. Das, M. K. As, V. Hamplpova and A. Bubnov, *J. Mol. Liq.*, 2019, **283**, 472–481.
83 N. Podoliak, M. Cigl, V. Hamplová, D. Pociecha and V. Novotná, *J. Mol. Liq.*, 2021, **336**, 116267.
84 H. Ocak, N. Y. Canli and B. Bilgin-Eran, *J. Mol. Struct.*, 2021, **1223**, 128975.
85 A. Özkonstanyan, H. H. Mert, M. S. Mert, B. Bilgin-Eran and H. Ocak, *J. Mol. Struct.*, 2020, **1222**, 128851.
86 K. K. Canon, *Jpn Pat.*, JP05078283 A, 1993.
87 E. Gomar-Nadal, C. Rovira and D. B. Amabilino, *Tetrahedron*, 2006, **62**, 3370–3379.
88 D. Güzeller, H. Ocak, B. Bilgin-Eran, M. Prehm and C. Tschierske, *J. Mater. Chem. C*, 2015, **3**, 4269–4282.
89 R. Adams and L. H. Ulich, *J. Am. Chem. Soc.*, 1920, **42**, 599–611.
90 J. L. Serrano, T. Sierra, Y. Gonzalez, C. Bolm, K. Weikardt, A. Magnus and G. Moll, *J. Am. Chem. Soc.*, 1995, **117**, 8312.
91 B. Neises and W. Steglich, *Angew. Chem., Int. Ed. Engl.*, 1978, **17**, 622.
92 A. Mori, M. Yokoo, M. Hashimoto, S. Ujiie, S. Diele, U. Baumeister and C. Tschierske, *J. Am. Chem. Soc.*, 2003, **125**, 6620–6621.
93 P. P. Crooker, in *Chirality in Liquid Crystals*, ed. H. S. Kitzerow and C. Bahr, Springer, New York, 2001, ch. 7, p. 186.
94 J. Pišljar, S. Ghosh, S. Turlapati, N. V. S. Rao, M. Škarabot, A. Mertelj, A. Petelin, A. Nych, M. Marincič, A. Pusovnik, M. Ravnik and I. Muševič, *Phys. Rev. X*, 2022, **12**, 011003.
95 T. Hirose and A. Yoshizawa, *J. Mater. Chem. C*, 2016, **4**, 8565–8574.
96 S. Taushanoff, K. V. Le, J. Williams, R. J. Twieg, B. K. Sadashiva, H. Takezoe and A. Jakli, *J. Mater. Chem.*, 2010, **20**, 5893–5898.
97 K. V. Le, S. Aya, Y. Sasaki, H. Choi, F. Araoka, K. Ema, J. Mieczkowski, A. Jakli, K. Ishikawa and H. Takezoe, *J. Mater. Chem.*, 2011, **21**, 2855–2857.
98 I.-H. Chiang, C.-J. Long, H.-C. Lin, W.-T. Chuang and J.-J. Lee, *ACS Appl. Mater. Interfaces*, 2014, **6**, 228–235.
99 (*a*) A. Baghla, M. Sahai, N. Yadav, S. P. Gupta, V. Manjuladevi, J. K. Vij and S. K. Pal, *Chem. Sci.*, 2025, **16**, 8002–8013; (*b*) R. Kumar Khan, B. Shivaranjini, S. Umadevi and R. Pratibha, *Chem. Phys.*, 2025, **602**, 113013.
100 R. K. Khan, *ChemPhysChem*, 2024, **25**, e202400779.
101 K. V. Le, M. Hafuri, H. Ocak, B. Bilgin-Eran, C. Tschierske and F. Araoka, *ChemPhysChem*, 2016, **17**, 1425–1429.
102 I. Dierking, *Liq. Cryst.*, 2025, DOI: **10.1080/02678292.2025.2517865**.
103 Y. Cao, M. Alaasar, L. Zhang, C. Zhu, C. Tschierske and F. Liu, *J. Am. Chem. Soc.*, 2022, **144**, 6936–6945.
104 E. Efrati and W. T. M. Irvine, *Phys. Rev. X*, 2014, **4**, 011003.
105 G. M. Grason, *Rev. Mod. Phys.*, 2015, **87**, 401–419.
106 E. Frezza, A. Ferrarini, H. B. Kolli, A. Giacometti and G. Cinacchi, *Phys. Chem. Chem. Phys.*, 2014, **16**, 16225–16232.
107 Y. Cao, M. Alaasar, A. Nallapaneni, M. Salamonczyk, P. Marinko, E. Gorecka, C. Tschierske, F. Liu, N. Vaupotič and C. Zhu, *Phys. Rev. Lett.*, 2020, **125**, 027801.
108 J. G. Fernsler, M. A. Glaser, R. Shao, D. A. Coleman, J. E. Maclennan, D. R. Link, C. Chang, K. Lanham, D. Walba, C. Boyer, J. A. Zasadzinski and N. A. Clark, *Liq. Cryst.*, 2017, **44**, 769–783.
109 R. J. Mandle, S. J. Cowling and J. W. Goodby, *Chem. – Eur. J.*, 2017, **23**, 14554–14562.
110 H. Nishikawa, K. Shiroshita, H. Higuchi, Y. Okumura, Y. Haseba, S.-I. Yamamoto, K. Sago and H. Kikuchi, *Adv. Mater.*, 2017, **29**, 1702354.
111 X. Chen, M. Shuai, B. Zhong, V. Martinez, E. Korblova, M. A. Glaser, J. E. Maclennan, D. M. Walba and N. A. Clark, *Proc. Natl. Acad. Sci. U. S. A.*, 2025, **122**, e2424917122.
112 B. Zhong, M. Shuai, X. Chen, V. Martinez, E. Korblova, M. A. Glaser, J. E. Maclennan and N. A. Clark, *Soft Matter*, 2025, **21**, 1122–1133.
113 R. K. Khan, *Appl. Res.*, 2025, **4**, e70018.

